Rapid Communications

Spontaneous ferromagnetism and finite surface energy gap in the topological insulator Bi_2Se_3 from surface Bi_{Se} antisite defects

Suhas Nahas,* Biplab Sanyal,† and Annica M. Black-Schaffer‡
Department of Physics and Astronomy, Uppsala University, Box 516, SE-751 20 Uppsala, Sweden

(Received 24 February 2020; accepted 13 October 2020; published 23 October 2020)

We perform *ab initio* calculations on Bi_{Se} antisite defects in the surface of Bi_2Se_3, finding strong low-energy defect resonances with a spontaneous ferromagnetism, fixed to an out-of-plane orientation due to an exceptionally large magnetic anisotropy energy. For antisite defects in the surface layer, we find semi-itinerant ferromagnetism and strong hybridization with the Dirac surface state, generating a finite energy gap. For deeper lying defects, such hybridization is largely absent, the magnetic moments become more localized, and no energy gap is present.

DOI: 10.1103/PhysRevB.102.140407

Topological insulators (TIs) [1,2] have been one of the most intensively studied areas in physics in the past decade, owing to their remarkable electronic properties: The bulk is insulating but the surfaces are metallic due to a gapless Dirac surface state (DSS) protected by time reversal symmetry (TRS).

Besides an interest in discovering new TIs, considerable effort has also been dedicated to opening up an energy gap in the DSS spectrum by breaking TRS, in order to enhance the electric control and also achieve the quantum anomalous Hall effect (QAHE) [3–5]. A natural route to break TRS is to introduce an effective magnetic field perpendicular to the surface of the TI [6]. Most of the studies along this route have involved doping the TI with magnetic impurities [6–15], whose magnetic moments might couple ferromagnetically through Ruderman-Kittel-Kasuya-Yosida (RKKY) [16,17], Van Vleck [18], or other exchange [11,12,19–21] mechanisms to produce the necessary out-of-plane magnetic field. A more recent development has been the realization of intrinsic magnetism in $MnBi_2Te_4$ [22–25], where the Mn atoms order antiferromagnetically with an out-of-plane magnetic anisotropy.

However, for both magnetic impurities in TI and $MnBi_2Te_4$, there seem to exist significant complications when it comes to opening a gap in the DSS, with experiments so far reporting both the presence of an energy gap [9,26–29] and finite density of states [30–39] at the Dirac point. Also, in the case of thin films, the hybridization between the two DSSs could be the reason for a finite energy gap [40–42], and not TRS breaking. For magnetic impurities, a two-fluid description has been proposed [43] to account for the contradicting results. Here, the DSS spectrum is indeed gapped due to TRS breaking, but at the same time the nonmagnetic part of the scattering potential produces localized impurity-induced resonances [44–48] filling up the gap [49].

In this Rapid Communication, we show that a surface energy gap is generated in the most common TI, Bi_2Se_3, from intrinsic Bi_{Se} antisite defects, entirely without the need for foreign magnetic atoms. By performing extensive *ab initio* calculations of antisite defects, we find defect-induced low-energy resonances, which spontaneously acquire a magnetic moment and thus gap the DSS. Antisite defects and their associated resonance states have already been observed experimentally using scanning tunneling microscopy (STM) [50–53], in both surface and subsurface layers, when growing Bi_2Se_3 in a Bi-rich environment [54–57]. An additional benefit of Bi_{Se} defects is that they behave as compensating *p*-type dopants, neutralizing the naturally occurring *n*-type Se vacancies by moving the Dirac point closer to the Fermi level [57,58].

In detail, we show how Bi_{Se} antisite defects in the TI surface produce low-energy states, with a spontaneous magnetization which even increases for lower concentrations. We find a magnetic anisotropy energy favoring an out-of-plane magnetic orientation of individual antisite defects that is two orders of magnitude larger than for common magnetic dopants. Together with an appreciable ferromagnetic exchange coupling this guarantees an out-of-plane ferromagnetic alignment between different defects. For antisite defects in the surface layer, we find semi-itinerant ferromagnetism and defect states coupling strongly to the DSS, resulting in a sizable energy gap in the DSS. On the other hand, antisite defects in the first subsurface layer display more localized magnetism with no discernible hybridization with the DSSs and consequently no DSS energy gap. This also reveals that a significant hybridization is necessary between the DSS and the defect states for the magnetic moment to be able to produce an energy gap. Taken together, our results open

*suhas.nahas@physics.uu.se
†biplab.sanyal@physics.uu.se
‡annica.black-schaffer@physics.uu.se

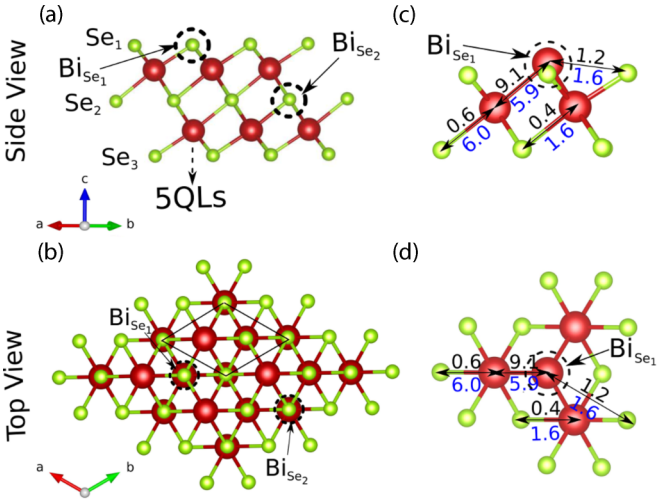

FIG. 1. (a) Side and (b) top views of the pristine Bi_2Se_3 slab, with Bi (Se) atoms in red (green) and the conventional lattice vectors of Bi_2Se_3 used as reference axes. The locations of Bi_{Se_1} and Bi_{Se_2} antisite defects are indicated by dotted circles and the surface unit cell of pristine Bi_2Se_3 by the black parallelogram. (c) Side and (d) top views of the neighborhood of the Bi_{Se_1} antisite defect with total relative (in %) bond length change in the presence (absence) of spin-orbit coupling in black (blue).

up a general pathway for designing magnetic and gapped TIs, by merely tuning the synthesizing conditions and thus completely avoiding the need for external magnetic impurity atoms.

Method. We perform electronic structure calculations, based on density functional theory (DFT), as implemented in the Vienna *ab initio* simulation package (VASP [59]), on Bi_2Se_3 slabs containing six quintuple layers (Se_1-Bi_1-Se_2-Bi_2-Se_3) in order to capture the TI surface, while still maintaining bulk conditions within the slab. On the surface we create a supercell by repeating the conventional surface unit cell, $n \times n$ ($n = 2, 3, 4$), adding one defect per supercell, resulting in defect concentrations $x \sim 25\%$, 11%, and 6%. Below we mainly report results for antisite defects $Bi_{Se_{1,2}}$, i.e., Bi replacing either the surface Se_1 or subsurface Se_2 atom [see Figs. 1(a) and 1(b)], but we also study Bi_{Se} defects in deeper layers, including the bulk. We carry out the structural and electronic optimizations using a plane-wave basis set with a kinetic energy cutoff 270 eV [60], together with projector augmented-wave (PAW) pseudopotentials. We use the generalized gradient approximation (GGA) for the exchange-correlation functional [61] and DFT-D3 [62] to properly account for the van der Waals corrections. Furthermore, we use a Γ-centered $k \times k \times 1$ grid to sample the Brillouin zone, where for even (odd) n we use $k \times n = 8(9)$ and $k \times n = 4(3)$ for the electronic and structural optimizations, respectively. We also use a 30-Å vacuum to isolate each periodic instance of the slab. In terms of convergence criteria, we use force and energy convergence thresholds of 10^{-6} eV (corresponding to 3×10^{-2} meV/Å) and 10^{-7} eV, respectively. We perform all calculations in a scalar relativistic manner, always including the effects of spin-orbit coupling, and also allow for a finite magnetization in all directions.

Structural distortions. We start by performing structural optimizations of the atomic positions for each defected TI surface. This both establishes the equilibrium positions of the Bi_{Se} defects and gives a structural view on the impact of antisite defects. To quantify the latter, we track the atomic distortions caused by the Bi_{Se} defects by comparing with an equivalently relaxed pristine TI slab. In Figs. 1(c) and 1(d) we display in black text the relative change of bond lengths (in %) in the neighborhood of the Bi_{Se_1} defect, while blue text reports the equivalent change when ignoring spin-orbit coupling. As seen, the Bi_{Se_1} defect creates large local perturbations of the lattice structure, with bond lengths changing as much as 9% for nearest-neighbor bonds. This is by all accounts a large structural change, which we at least partly can attribute to the 40% larger atomic size of the Bi atom compared to Se. In comparison, the next-nearest-neighbor bonds show almost negligible distortion. If we were to ignore the spin-orbit coupling in the structural optimization, we find that both the nearest- and next-nearest-neighbor bond show a similar change. This illustrates that spin-orbit coupling is essential to capture not just the DSS but also the correct atomic structure of antisite defects in TIs. We find similar structural patterns for the other antisite defects, including defects in the bulk of the TI [see Supplemental Material (SM) [63]].

Magnetism. We next turn to the electronic properties of antisite defects. Surprisingly, we find that Bi_2Se_3 with antisite surface defects hosts a pronounced magnetization, despite the intrinsically nonmagnetic nature of antisite defects. For both Bi_{Se_1} and Bi_{Se_2}, we observe a highly anisotropic, out-of-plane (c-direction), magnetization. Bi_{Se_3} (Bi on the third Se layer) also gives rise to a net magnetization, but the defect also easily migrates to the van der Waals gap during structural optimization. For antisite defects further into the bulk we find no magnetization. Interestingly, if we start with atomic structures optimized *without* spin-orbit coupling, we find no net magnetization for antisite defects in any layer, including $Bi_{Se_{1,2}}$. Thus, the large structural distortions caused by spin-orbit coupling are crucial for correctly determining the electronic ground state of antisite defects.

In Fig. 2(a) we show how the net magnetization varies as a function of defect concentration for the Bi_{Se_1} and Bi_{Se_2} defects. We find that both spin and orbital moments increase with decreasing concentration: The surface Bi_{Se_1} defect shows an almost threefold increase in the spin magnetic moment when decreasing the defect concentration from 25% to 6% (see SM [63]), while the subsurface Bi_{Se_2} defect shows a minor increase. The increasing, and persistent, magnetization with decreasing defect concentrations assures that the magnetization is stable in the dilute defect limit. In Fig. 2(a) we also see that the orbital moments are large, strongly suggestive of a highly anisotropic magnetization [64–67]. In order to confirm this, we calculate the magnetic anisotropy energy (MAE), i.e., the total energy difference between out-of-plane and in-plane magnetizations. Figure 2(b) shows how also the MAE increases significantly with decreasing defect concentration. Notably, the MAE is almost 20 (12) meV for the $Bi_{Se_{1(2)}}$ antisite defect at the lowest concentration. Such MAE values are impressive, about two orders of magnitude larger than what has been achieved in TIs with the magnetic transition metal impurities Cr, V, or Mn, where the MAE is

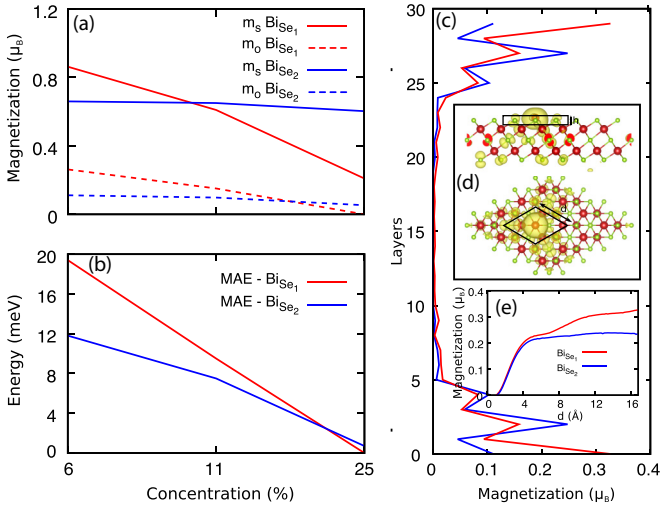

FIG. 2. (a) Magnetization, spin m_s (solid) and orbital m_o (dashed), and (b) MAE for Bi_{Se_1} (red) and Bi_{Se_2} (blue) antisite defects as a function of defect concentration. (c) Layer-resolved spin magnetization for each atomic layer for 6% Bi_{Se_1} (red) and Bi_{Se_2} (blue) antisite defects. (d) Real-space magnetization density in the first surface layer for the Bi_{Se_1} defect with isovalue 0.1 times the maximum. (e) Integrated spin magnetization for Bi_{Se_1} (red) and Bi_{Se_2} (blue) defects over the volume of the black rhombus displayed in (d) (centered at the antisite defect with side d and thickness h), given as a function of d with h equal to the Bi-Se c-axis projected bond length.

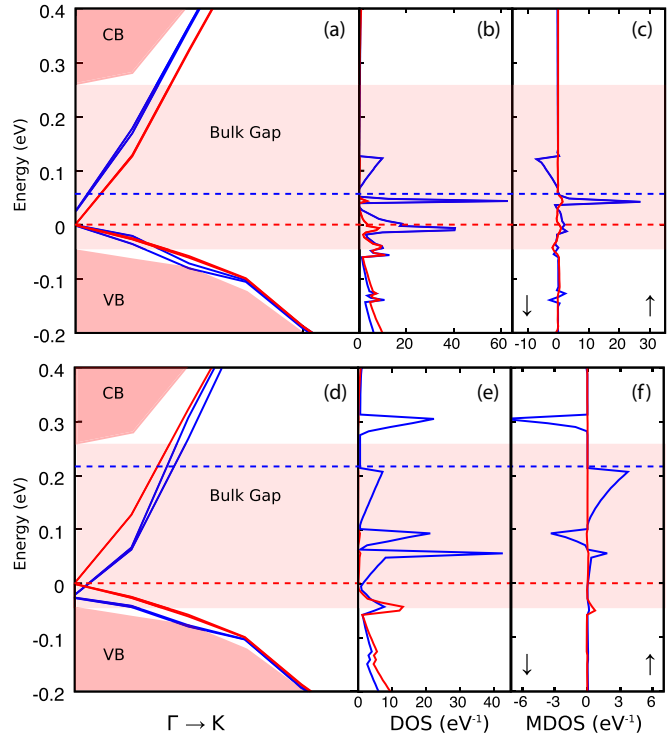

FIG. 3. (a), (d) Band structure along Γ-K for pristine (red) and Bi_{Se_1} (a) and Bi_{Se_2} (d) 6% defected (blue) TI system with defect states removed. Bulk conduction and valence bands (dark pink) are aligned to create a common bulk band gap (light pink), with the Fermi level (dotted lines) in the pristine system set to 0 eV. (b), (e) Complete density of states (DOS) and (c), (f) magnetization density of states (MDOS) in the bulk (red) and the surface quintuple layer (blue) for the defected systems.

only of the order of 0.1 meV [68]. We also directly calculate the exchange coupling as the energy difference between ferromagnetic and antiferromagnetic c-axis alignments of two Bi_{Se_1} defects at a distance of ∼14.5 Å and ∼6% concentration (see SM [63]). We find the ferromagnetic configuration to be lower in energy by 3.6 meV. This is a large value considering the distance between the defects and contributes by a large amount (∼500 meV Å^2) [69] to the spin stiffness as predicted for spontaneous magnetization [70,71]. Together with the large MAE, it also gives an exceptionally strong preference for an out-of-plane ferromagnetic alignment (with a large Curie temperature) of the antisite magnetic moments, thus creating optimal conditions for also opening a gap in the DSS [6,72,73].

To further understand the antisite-induced magnetic state, we analyze its spatial properties in the 6% $Bi_{Se_{1,2}}$ systems. In Fig. 2(c) we resolve the spin magnetic moments into layers of thickness h equal to the Bi-Se bond length projected onto the c axis [see the black box in Fig. 2(d)]. We find that magnetism is only present in the surface layers, with a peak in the layer of the defect. For the in-plane behavior we show in Fig. 2(d) the real-space magnetization density of the surface atoms for the Bi_{Se_1} defect. We find that the magnetization is semi-itinerant, extending with a threefold spatial pattern from the defect to distances well beyond the primary unit cell. To quantify the itinerancy, we study how the magnetization accumulates with distance away from the antisite defect. For this we plot in Fig. 2(e) the net magnetization within a rhombus with the same shape as the unit cell and with thickness h and centered around the antisite defect with varying side length d. For Bi_{Se_1} the magnetization continuously increases with d, demonstrating semi-itinerancy. However, for the Bi_{Se_2} defect we find that the magnetization is localized since a plateau develops when d equals about a quarter of the lattice parameter of the unit cell in the a-b plane.

Surface energy gap. Having established finite magnetism from intrinsically nonmagnetic Bi_{Se} defects, we turn to investigating the electronic spectrum in detail. Since we find an exceptionally strong MAE, effectively guaranteeing an out-of-plane magnetic moment, we are particularly interested in how the magnetization affects the topologically protected DSSs in Bi_2Se_3. In Fig. 3(a) we plot the band dispersion along the Γ-K direction for the Bi_{Se_1} defect system at 6% concentration (blue) and compare it with the equivalent but defect-free system (red). To be able to effectively compare the two systems, we first set the Fermi level of the pristine slab to 0 eV at the Dirac point. We then align the spectrum of the defected slab such that the valence (VB) and conduction (CB) bands perfectly align for the defect and defect-free systems (see SM [63]). This is possible since both systems reach bulk conditions in the interior of the slabs. We refrain from plotting all bands belonging to the bulk but instead conceptually show their extent in the dark pink regions. We see a clear bulk band gap ranging from −0.05 to 0.27 eV (light pink), in agreement with previous predictions [74]. We also identify an intrinsic doping produced by the antisite defect, as the Fermi level

(dotted lines) of the antisite defect system falls at a slightly higher energy (61 meV with 6% defects).

We next focus on the in-gap region, where we expect to find the DSS, but also defect states generated by the antisite defects. Initially we are interested only in the intrinsic DSSs, and therefore first exclude all bands belonging to the antisite defects. We can do this easily beyond the Γ point, as there the DSS and the antisite defect states have very different orbital and spatial characters: States belonging to the DSS are present throughout the surface, while the antisite defect states are heavily localized at the defect. At the Γ point we find finite hybridization between the DSS and some defect states, but, nonetheless, we can still remove the defect states based on their orbital weights and flat energy dispersion (due to their localization) (see SM [63]). In this way we extract and plot only the DSSs for the Bi_{Se_1} defect in Fig. 3(a). The DSSs in the pristine system (red) and antisite system (blue) are very similar at higher energies, both showing a linear Dirac spectrum with the same slope. However, at low energies we find a clear 24 meV energy gap induced in the antisite system. The gap size at the Γ point is fully consistent with the slope of the DSS at higher energies. In Fig. 3(d) we plot the equivalent bands for the Bi_{Se_2} defect, but here the DSS energy gap is negligible, despite the finite magnetization. This is another property, along with the spatial extent of the magnetization, where we observe contrasting behavior for Bi_{Se_1} and Bi_{Se_2} defects.

Density of states. To gain further insight into the magnetization and DSS energy gap we investigate the density of states (DOS). In Figs. 3(b) and 3(e) we compare the DOS in the bulk (red) with that of the surface quintuple layer of the Bi_{Se_1} and Bi_{Se_2} antisite systems (blue), respectively. By comparing these two DOS, we find that the DOS predominantly belonging to the $Bi_{Se_{1(2)}}$ antisite defect occupies an energy window ranging from around −20 (0) to 120 (220) meV, with respect to the pristine Dirac point, thus filling a large part of the bulk energy gap for both types of defects. However, we also observe that the defect states coexist (in energy) with the induced energy gap for the Bi_{Se_1} defect, while for the Bi_{Se_2} defect, the defect states are mainly around 60 meV above the Dirac point of that defected system. By additionally studying the orbital character of all low-energy bands near the Γ point, we find that the nondispersive Bi_{Se_1} states overlapping in energy with the Dirac point strongly hybridize with the DSS (see SM [63]). This hybridization explains why the Bi_{Se_1} defect both generates a semi-itinerant magnetization and opens an energy gap in the DSS by effectively acting as a TRS breaking perturbation on the DSS. The strong hybridization between the magnetic Bi_{Se_1} defect states and the DSS also provides the necessary pathway for a strong exchange coupling to align the antisite magnetic moments [75]. Here, with Bi_{Se} being an inherent defect, it naturally has the same (s, p) orbital character as the DSS. This provides an additional clear advantage, beyond the energy overlap, in generating a strong exchange coupling over transition metal atoms with their d orbital character [68].

The semi-itinerant magnetism and finite energy gap for the Bi_{Se_1} system should be contrasted with the behavior of the Bi_{Se_2} system. While the Bi_{Se_2} defect states have a finite magnetization, they have a negligible overlap in energy with the DSS around its Dirac point. As a consequence, they do not effectively couple to the DSS and thus the magnetization stays localized and the energy gap in the DSS remains vanishingly small. Thus we conclude that the mere presence of an out-of-plane magnetic defect moment does not guarantee the opening up of an energy gap in TIs, but that an effective coupling between the magnetic defect states and the DSS needs to be present as well.

The creation of in-gap defect-induced resonance states for strong potential defects has previously been established for generic 2D Dirac materials [48], including the DSS in TIs [45] and also in the presence of finite magnetic moments [49]. Our *ab initio* results establish that naturally occurring surface antisite Bi_{Se} defects act as such strong potential scatterers, inducing in-gap resonance states. This then also implies a so-called two-fluid behavior [43], with both the dispersive DSS and the localized impurity resonance states filling the TI bulk energy gap, as is clearly visible in Fig. 3.

Finally, we compare the magnetization density of states (MDOS) between the bulk and surface in Figs. 3(c) and 3(f) for the $Bi_{Se_{1,2}}$ defects. We find that the magnetization in the system is almost exclusively associated with the in-gap defect states. This also finally offers an explanation as to why the antisite defect states spontaneously become magnetized in the first place: The defect resonance states generate a large DOS at the Fermi level $\rho(E_F)$, which necessarily becomes prone to spontaneous magnetization. In its simplest incarnation the instability towards magnetism is given by a Stoner-like criterion $\rho(E_F)U > 1$, where U is the electron-electron interaction strength [76]. Our *ab initio* results on antisite Bi_{Se} defects on the surface of the TI Bi_2Se_3 show that antisite defects are indeed strong enough potential scatterers to generate these low-energy defect-induced resonances, which then, owing to the finite exchange interactions in the TI, also become spontaneously magnetized (see SM for further information [63]). Moreover, naturally occurring Se vacancy states will not be detrimental as they appear at a larger energy [45,52].

Conclusions. Our fully relativistic *ab initio* calculations show that intrinsic antisite Bi_{Se} defects in the surface layer of the TI Bi_2Se_3 generate a finite energy gap in the topologically protected DSSs. The antisite defect produces low-energy resonance states, which spontaneously become magnetic with an exceptionally large MAE guaranteeing an out-of-plane magnetic moment. With the defect states also overlapping in energy with the Dirac point, they hybridize with the DSS and thus the surface antisite defect acts as an effective magnetic field opening an energy gap in the DSS. For antisite defects buried in the first subsurface layer we also find a finite magnetization, but the overlap with the DSS is negligible and thus no measurable energy gap is present in the DSS. These results illustrate both that naturally occurring defects can produce a magnetic TI and that magnetic defect moments require effective coupling to the DSS to open an energy gap. Moreover, the results provide an important observation on the site dependence of defects in exhibiting the essential physics of TIs.

Acknowledgments. We thank A. Bouhon, X. Chen, R. Esteban-Puyuelo, B. Ghosh, M. Mashkoori, F. Parhizgar, and D. Wang for fruitful discussions. This work was supported by the Swedish Research Council (Vetenskapsrådet, Grants

No. 2014-3721 and No. 2018-03488), the Swedish Foundation for Strategic Research (SSF), and the Wallenberg Academy Fellows program through the Knut and Alice Wallenberg Foundation. The simulations were performed on resources provided by the Swedish National Infrastructure for Computing (SNIC) at HPC2N, NSC, PDC, and UPPMAX.

[1] M. Z. Hasan and C. L. Kane, Rev. Mod. Phys. **82**, 3045 (2010).
[2] X.-L. Qi and S.-C. Zhang, Rev. Mod. Phys. **83**, 1057 (2011).
[3] F. D. M. Haldane, Phys. Rev. Lett. **61**, 2015 (1988).
[4] M. Onoda and N. Nagaosa, Phys. Rev. Lett. **90**, 206601 (2003).
[5] C.-X. Liu, X.-L. Qi, X. Dai, Z. Fang, and S.-C. Zhang, Phys. Rev. Lett. **101**, 146802 (2008).
[6] Y. Tokura, K. Yasuda, and A. Tsukazaki, Nat. Rev. Phys. **1**, 126 (2019).
[7] Y. S. Hor, P. Roushan, H. Beidenkopf, J. Seo, D. Qu, J. G. Checkelsky, L. A. Wray, D. Hsieh, Y. Xia, S.-Y. Xu, D. Qian, M. Z. Hasan, N. P. Ong, A. Yazdani, and R. J. Cava, Phys. Rev. B **81**, 195203 (2010).
[8] R. Yu, W. Zhang, H.-J. Zhang, S.-C. Zhang, X. Dai, and Z. Fang, Science **329**, 61 (2010).
[9] C.-Z. Chang, J. Zhang, X. Feng, J. Shen, Z. Zhang, M. Guo, K. Li, Y. Ou, P. Wei, L.-L. Wang, Z.-Q. Ji, Y. Feng, S. Ji, X. Chen, J. Jia, X. Dai, Z. Fang, S.-C. Zhang, K. He, Y. Wang *et al.*, Science **340**, 167 (2013).
[10] C.-Z. Chang, W. Zhao, D. Y. Kim, H. Zhang, B. A. Assaf, D. Heiman, S.-C. Zhang, C. Liu, M. H. W. Chan, and J. S. Moodera, Nat. Mater. **14**, 473 (2015).
[11] T. R. F. Peixoto, H. Bentmann, S. Schreyeck, M. Winnerlein, C. Seibel, H. Maaß, M. Al-Baidhani, K. Treiber, S. Schatz, S. Grauer, C. Gould, K. Brunner, A. Ernst, L. W. Molenkamp, and F. Reinert, Phys. Rev. B **94**, 195140 (2016).
[12] W. Zhang, D. West, S. H. Lee, Y. Qiu, C.-Z. Chang, J. S. Moodera, Y. S. Hor, S. Zhang, and W. Wu, Phys. Rev. B **98**, 115165 (2018).
[13] W. Liu, Y. Xu, L. He, G. van der Laan, R. Zhang, and K. Wang, Sci. Adv. **5**, eaav2088 (2019).
[14] A. J. Bestwick, E. J. Fox, X. Kou, L. Pan, K. L. Wang, and D. Goldhaber-Gordon, Phys. Rev. Lett. **114**, 187201 (2015).
[15] X. Kou, S.-T. Guo, Y. Fan, L. Pan, M. Lang, Y. Jiang, Q. Shao, T. Nie, K. Murata, J. Tang, Y. Wang, L. He, T.-K. Lee, W.-L. Lee, and K. L. Wang, Phys. Rev. Lett. **113**, 137201 (2014).
[16] D. A. Abanin and D. A. Pesin, Phys. Rev. Lett. **106**, 136802 (2011).
[17] J.-J. Zhu, D.-X. Yao, S.-C. Zhang, and K. Chang, Phys. Rev. Lett. **106**, 097201 (2011).
[18] M. Li, C.-Z. Chang, L. Wu, J. Tao, W. Zhao, M. H. W. Chan, J. S. Moodera, J. Li, and Y. Zhu, Phys. Rev. Lett. **114**, 146802 (2015).
[19] M. G. Vergniory, M. M. Otrokov, D. Thonig, M. Hoffmann, I. V. Maznichenko, M. Geilhufe, X. Zubizarreta, S. Ostanin, A. Marmodoro, J. Henk, W. Hergert, I. Mertig, E. V. Chulkov, and A. Ernst, Phys. Rev. B **89**, 165202 (2014).
[20] M. Ye, T. Xu, G. Li, S. Qiao, Y. Takeda, Y. Saitoh, S.-Y. Zhu, M. Nurmamat, K. Sumida, Y. Ishida, S. Shin, and A. Kimura, Phys. Rev. B **99**, 144413 (2019).
[21] A. Tcakaev, V. B. Zabolotnyy, R. J. Green, T. R. F. Peixoto, F. Stier, M. Dettbarn, S. Schreyeck, M. Winnerlein, R. C. Vidal, S. Schatz, H. B. Vasili, M. Valvidares, K. Brunner, C. Gould, H. Bentmann, F. Reinert, L. W. Molenkamp, and V. Hinkov, Phys. Rev. B **101**, 045127 (2020).
[22] J. Li, Y. Li, S. Du, Z. Wang, B.-L. Gu, S.-C. Zhang, K. He, W. Duan, and Y. Xu, Sci. Adv. **5**, eaaw5685 (2019).
[23] D. Zhang, M. Shi, T. Zhu, D. Xing, H. Zhang, and J. Wang, Phys. Rev. Lett. **122**, 206401 (2019).
[24] A. Zeugner, F. Nietschke, A. U. B. Wolter, S. Gaß, R. C. Vidal, T. R. F. Peixoto, D. Pohl, C. Damm, A. Lubk, R. Hentrich, S. K. Moser, C. Fornari, C. H. Min, S. Schatz, K. Kißner, M. Ünzelmann, M. Kaiser, F. Scaravaggi, B. Rellinghaus, K. Nielsch *et al.*, Chem. Mater. **31**, 2795 (2019).
[25] Y. Gong, J. Guo, J. Li, K. Zhu, M. Liao, X. Liu, Q. Zhang, L. Gu, L. Tang, X. Feng, D. Zhang, W. Li, C. Song, L. Wang, P. Yu, X. Chen, Y. Wang, H. Yao, W. Duan, Y. Xu *et al.*, Chin. Phys. Lett. **36**, 076801 (2019).
[26] J. Sánchez-Barriga, A. Varykhalov, G. Springholz, H. Steiner, R. Kirchschlager, G. Bauer, O. Caha, E. Schierle, E. Weschke, A. A. Ünal, S. Valencia, M. Dunst, J. Braun, H. Ebert, J. Minár, E. Golias, L. V. Yashina, A. Ney, V. Holý, and O. Rader, Nat. Commun. **7**, 10559 (2016).
[27] M. M. Otrokov, I. I. Klimovskikh, H. Bentmann, D. Estyunin, A. Zeugner, Z. S. Aliev, S. Gaß, A. U. B. Wolter, A. V. Koroleva, A. M. Shikin, M. Blanco-Rey, M. Hoffmann, I. P. Rusinov, A. Y. Vyazovskaya, S. V. Eremeev, Y. M. Koroteev, V. M. Kuznetsov, F. Freyse, J. Sánchez-Barriga, I. R. Amiraslanov *et al.*, Nature (London) **576**, 416 (2019).
[28] Y. L. Chen, J.-H. Chu, J. G. Analytis, Z. K. Liu, K. Igarashi, H.-H. Kuo, X. L. Qi, S. K. Mo, R. G. Moore, D. H. Lu, M. Hashimoto, T. Sasagawa, S. C. Zhang, I. R. Fisher, Z. Hussain, and Z. X. Shen, Science **329**, 659 (2010).
[29] L. A. Wray, S.-Y. Xu, Y. Xia, D. Hsieh, A. V. Fedorov, Y. S. Hor, R. J. Cava, A. Bansil, H. Lin, and M. Z. Hasan, Nat. Phys. **7**, 32 (2011).
[30] T. Valla, Z.-H. Pan, D. Gardner, Y. S. Lee, and S. Chu, Phys. Rev. Lett. **108**, 117601 (2012).
[31] M. R. Scholz, J. Sánchez-Barriga, D. Marchenko, A. Varykhalov, A. Volykhov, L. V. Yashina, and O. Rader, Phys. Rev. Lett. **108**, 256810 (2012).
[32] H. Li, S.-Y. Gao, S.-F. Duan, Y.-F. Xu, K.-J. Zhu, S.-J. Tian, J.-C. Gao, W.-H. Fan, Z.-C. Rao, J.-R. Huang, J.-J. Li, D.-Y. Yan, Z.-T. Liu, W.-L. Liu, Y.-B. Huang, Y.-L. Li, Y. Liu, G.-B. Zhang, P. Zhang, T. Kondo *et al.*, Phys. Rev. X **9**, 041039 (2019).
[33] Y.-J. Hao, P. Liu, Y. Feng, X.-M. Ma, E. F. Schwier, M. Arita, S. Kumar, C. Hu, R. Lu, M. Zeng, Y. Wang, Z. Hao, H.-Y. Sun, K. Zhang, J. Mei, N. Ni, L. Wu, K. Shimada, C. Chen, Q. Liu, and C. Liu, Phys. Rev. X **9**, 041038 (2019).
[34] Y. J. Chen, L. X. Xu, J. H. Li, Y. W. Li, H. Y. Wang, C. F. Zhang, H. Li, Y. Wu, A. J. Liang, C. Chen, S. W. Jung, C. Cacho, Y. H. Mao, S. Liu, M. X. Wang, Y. F. Guo, Y. Xu, Z. K. Liu, L. X. Yang, and Y. L. Chen, Phys. Rev. X **9**, 041040 (2019).
[35] T. Schlenk, M. Bianchi, M. Koleini, A. Eich, O. Pietzsch, T. O. Wehling, T. Frauenheim, A. Balatsky, J.-L. Mi, B. B. Iversen,

J. Wiebe, A. A. Khajetoorians, P. Hofmann, and R. Wiesendanger, Phys. Rev. Lett. **110**, 126804 (2013).
[36] H. Beidenkopf, P. Roushan, J. Seo, L. Gorman, I. Drozdov, Y. S. Hor, R. J. Cava, and A. Yazdani, Nat. Phys. **7**, 939 (2011).
[37] P. Sessi, F. Reis, T. Bathon, K. A. Kokh, O. E. Tereshchenko, and M. Bode, Nat. Commun. **5**, 5349 (2014).
[38] F. Yang, Y. R. Song, H. Li, K. F. Zhang, X. Yao, C. Liu, D. Qian, C. L. Gao, and J.-F. Jia, Phys. Rev. Lett. **111**, 176802 (2013).
[39] Y. Okada, C. Dhital, W. Zhou, E. D. Huemiller, H. Lin, S. Basak, A. Bansil, Y.-B. Huang, H. Ding, Z. Wang, S. D. Wilson, and V. Madhavan, Phys. Rev. Lett. **106**, 206805 (2011).
[40] J. Linder, T. Yokoyama, and A. Sudbø, Phys. Rev. B **80**, 205401 (2009).
[41] H.-Z. Lu, W.-Y. Shan, W. Yao, Q. Niu, and S.-Q. Shen, Phys. Rev. B **81**, 115407 (2010).
[42] C.-X. Liu, H. J. Zhang, B. Yan, X.-L. Qi, T. Frauenheim, X. Dai, Z. Fang, and S.-C. Zhang, Phys. Rev. B **81**, 041307(R) (2010).
[43] P. Sessi, R. R. Biswas, T. Bathon, O. Storz, S. Wilfert, A. Barla, K. A. Kokh, O. E. Tereshchenko, K. Fauth, M. Bode, and A. V. Balatsky, Nat. Commun. **7**, 12027 (2016).
[44] R. R. Biswas and A. V. Balatsky, Phys. Rev. B **81**, 233405 (2010).
[45] A. M. Black-Schaffer and A. V. Balatsky, Phys. Rev. B **85**, 121103(R) (2012).
[46] A. M. Black-Schaffer and A. V. Balatsky, Phys. Rev. B **86**, 115433 (2012).
[47] Z. Alpichshev, R. R. Biswas, A. V. Balatsky, J. G. Analytis, J.-H. Chu, I. R. Fisher, and A. Kapitulnik, Phys. Rev. Lett. **108**, 206402 (2012).
[48] T. Wehling, A. Black-Schaffer, and A. Balatsky, Adv. Phys. **63**, 1 (2014).
[49] A. M. Black-Schaffer, A. V. Balatsky, and J. Fransson, Phys. Rev. B **91**, 201411(R) (2015).
[50] S. Urazhdin, D. Bilc, S. H. Tessmer, S. D. Mahanti, T. Kyratsi, and M. G. Kanatzidis, Phys. Rev. B **66**, 161306(R) (2002).
[51] S. Kim, M. Ye, K. Kuroda, Y. Yamada, E. E. Krasovskii, E. V. Chulkov, K. Miyamoto, M. Nakatake, T. Okuda, Y. Ueda, K. Shimada, H. Namatame, M. Taniguchi, and A. Kimura, Phys. Rev. Lett. **107**, 056803 (2011).
[52] C. Mann, D. West, I. Miotkowski, Y. P. Chen, S. Zhang, and C.-K. Shih, Nat. Commun. **4**, 2277 (2013).
[53] J. Dai, D. West, X. Wang, Y. Wang, D. Kwok, S.-W. Cheong, S. B. Zhang, and W. Wu, Phys. Rev. Lett. **117**, 106401 (2016).
[54] J.-M. Zhang, W. Zhu, Y. Zhang, D. Xiao, and Y. Yao, Phys. Rev. Lett. **109**, 266405 (2012).
[55] D. West, Y. Y. Sun, H. Wang, J. Bang, and S. B. Zhang, Phys. Rev. B **86**, 121201(R) (2012).
[56] D. O. Scanlon, P. D. C. King, R. P. Singh, A. de la Torre, S. M. Walker, G. Balakrishnan, F. Baumberger, and C. R. A. Catlow, Adv. Mater. **24**, 2154 (2012).
[57] L. Xue, P. Zhou, C. X. Zhang, C. Y. He, G. L. Hao, L. Z. Sun, and J. X. Zhong, AIP Adv. **3**, 052105 (2013).
[58] Y. S. Hor, A. Richardella, P. Roushan, Y. Xia, J. G. Checkelsky, A. Yazdani, M. Z. Hasan, N. P. Ong, and R. J. Cava, Phys. Rev. B **79**, 195208 (2009).
[59] G. Kresse and J. Furthmüller, Phys. Rev. B **54**, 11169 (1996).
[60] We have checked that increasing the kinetic energy cutoff to 600 eV does not change the results for the 11%$Bi_{Se_{1,2}}$ defect.
[61] K. Shirali, W. A. Shelton, and I. Vekhter, arXiv:1905.01269.
[62] S. Grimme, J. Antony, S. Ehrlich, and H. Krieg, J. Chem. Phys. **132**, 154104 (2010).
[63] See Supplemental Material at http://link.aps.org/supplemental/10.1103/PhysRevB.102.140407 for details related to structural distortions around Bi_{Se_2} defects, pair-wise interactions between Bi_{Se_1} defects, alignment of pristine and defected band-structures, extraction of the DSS gap and MDOS at 6% and 25% Bi_{Se_1} concentrations.
[64] P. Bruno, Phys. Rev. B **39**, 865 (1989).
[65] R. Skomski, A. Kashyap, and A. Enders, J. Appl. Phys. **109**, 07E143 (2011).
[66] I. G. Rau, S. Baumann, S. Rusponi, F. Donati, S. Stepanow, L. Gragnaniello, J. Dreiser, C. Piamonteze, F. Nolting, S. Gangopadhyay, O. R. Albertini, R. M. Macfarlane, C. P. Lutz, B. A. Jones, P. Gambardella, A. J. Heinrich, and H. Brune, Science **344**, 988 (2014).
[67] X. Ou, H. Wang, F. Fan, Z. Li, and H. Wu, Phys. Rev. Lett. **115**, 257201 (2015).
[68] M. F. Islam, C. M. Canali, A. Pertsova, A. Balatsky, S. K. Mahatha, C. Carbone, A. Barla, K. A. Kokh, O. E. Tereshchenko, E. Jiménez, N. B. Brookes, P. Gargiani, M. Valvidares, S. Schatz, T. R. F. Peixoto, H. Bentmann, F. Reinert, J. Jung, T. Bathon, K. Fauth, M. Bode, and P. Sessi, Phys. Rev. B **97**, 155429 (2018).
[69] M. Pajda, J. Kudrnovský, I. Turek, V. Drchal, and P. Bruno, Phys. Rev. B **64**, 174402 (2001).
[70] D. M. Edwards and M. I. Katsnelson, J. Phys.: Condens. Matter **18**, 7209 (2006).
[71] O. V. Yazyev and M. I. Katsnelson, Phys. Rev. Lett. **100**, 047209 (2008).
[72] K. Nomura and N. Nagaosa, Phys. Rev. Lett. **106**, 166802 (2011).
[73] J. G. Checkelsky, J. Ye, Y. Onose, Y. Iwasa, and Y. Tokura, Nat. Phys. **8**, 729 (2012).
[74] H. Zhang, C.-X. Liu, X.-L. Qi, X. Dai, Z. Fang, and S.-C. Zhang, Nat. Phys. **5**, 438 (2009).
[75] M. R. Mahani, A. Pertsova, M. F. Islam, and C. M. Canali, Phys. Rev. B **90**, 195441 (2014).
[76] A. M. Black-Schaffer and D. Yudin, Phys. Rev. B **90**, 161413(R) (2014).